Analysing Fibre Composite Designs for High-Solidity Ducted Tidal Turbine Blades

Mitchell G. Borg
Department of Naval Architecture, Ocean, and Marine Engineering
University of Strathclyde
Glasgow, Scotland, United Kingdom
mitchell.borg@strath.ac.uk

Qing Xiao
Department of Naval Architecture, Ocean, and Marine Engineering
University of Strathclyde
Glasgow, Scotland, United Kingdom
qing.xiao@strath.ac.uk

Steven Allsop
Industrial Doctoral Centre for Offshore Renewable Energy (IDCORE)
University of Edinburgh
Edinburgh, Scotland, United Kingdom

Atilla Incecik
Department of Naval Architecture, Ocean, and Marine Engineering
University of Strathclyde
Glasgow, Scotland, United Kingdom

Christophe Peyrard
Electricité de France, Research and Development
EDF R&D
Chatou, Ile-de-France, France
christophe.peyrard@edf.fr

***Abstract*— This study elaborates a one-way fluid-structure interaction numerical model utilised in investigating the structural mechanics concerning the rotor blades comprising a ducted high-solidity tidal turbine. Coupling hydrodynamic outcomes as structural inputs in effort of acknowledging the most applicable setup, distinct designs are investigated, solid blades and cored blades, utilising fibre-reinforced composite materials, analysed within criteria related to blade axial deformation, induced radial strains, and rotor specific mass.**

***Index Terms*—high-solidity blades, fluid-structure interaction, FSI, CFD, FEA, composites, ducted turbine**

I. Introduction

Efforts to increase the efficiency of energy-generating turbines have been in constant development following their introduction to the global market [1]. At the forefront of the pertinent research is the increase of mass flow through the turbine, along with the alignment of the flow to facilitate further turbine installations. As a result of the research and development established, two conventional classifications of installations have been implemented around the blades of a turbine: bidirectional ducts and unidirectional ducts. Illustrated in Fig. 1, the two systems have been considered in significantly enhancing the performance of a turbine by increasing the flow velocity along the turbine.

Albeit the potential improvements, the performance capacity of bidirectional ducts is inadequately understood. A number of commercial endeavours have attempted in implementing the technology to achieve economic prospects, yet a substantial quantity have resulted in abandonment [1]. From the prospects, OpenHydro Ltd., considered amongst the more fruitful, had achieved commissionable and operational status with an open-centre ducted design approach [2] [3]. This setup employs an aperture at the centre of the turbine, hence not only utilising the duct as a flow modifier, but also as a unit in which the power generating system may be housed.

Instigative analyses assessing the effectivity of shrouded turbines have been directed by numerical methodologies. Werle and Presz [4] attained numerical validation in effort of developing a theoretical basis of the potential improvements available from ducted flow configurations. Fleming and Willden [5] investigated the difference in velocity through the throat of a bidirectional duct in accordance with distinctive duct profiles, where the implemented turbine was represented as an actuator disc utilising computational fluid dynamics (CFD).

In continuation, Belloni et al. [6] investigated the effects of different bidirectional duct setups utilising a coupled BEM-CFD method, whereas Allsop et al. [7] developed a numerical BEMT model to analyse flow through a duct. Shives and Crawford [8] analysed a ducted actuator disc model implementing CFD by varying the angle of attack of a unidirectional duct profile. In comparing two methodologies to impose numerical turbulence, Reynolds-averaged Navier-Stokes (RANS) and large eddy simulation (LES), Ahmed et al. [9] acknowledged the ineptness of resolving the wake by means of RANS-CFD. Holst et al. [10] conducted a numerical study to analyse the wave-induced loads on tidal turbine blades at distinct angles of attack; this was compared to blade-element momentum theory (BEMT) analyses, which depicted similar parameter outcomes.

Shultz et al. [11] established the reduction of a rotor power output to be systematic to the yaw angle of the free-stream in the analysis of a 2.4 MW turbine within a yaw angle range of -50^o and 50^o at two distinct free-stream velocities. The deflection of the wake as a result of the inflow was additionally investigated by comparing the deflection angles, deducing a relating factor between wake deflection and turbine load asymmetry. Suzuki [12] depicted a similar occurrence in numerically analysing two-bladed horizontal-axis turbines. Within a yaw angle range of 0^o to 45^o, a consistent decrease in power was observed, with a maximum deficiency of more

than 30% in peak power attainment at a bearing of 45^o.

McWilliam et al. [13] proposed a blade element momentum (BEM) model for yawed turbine flows with use of correction factors. Potential flow methodology terms were implemented within a range of operational conditions of a flow field, attaining better accuracy than conventional BEM, yet preserving its efficiency. Morote [14] presented a novel approach in deriving the effective angle of attack for rotor blades under swept flow conditions at yaw angles.

Albeit the commodious applicability of numerical hydrodynamic analysis for the evaluation of tidal turbines, the relevant methodologies typically consider the assumption of the rotor structure to be wholly rigid; upon physical implementation, however, this fails to hold. Munoz et al. [15] acknowledged the imperative of material selection in blade design in consequence of high deflection experienced by rotor blades fabricated from low rigidity materials, bringing about a significant reduction in rotor power generation. Amongst the more common materials utilised for tidal turbine rotor designs are composite materials, specifically glass-fibre reinforced polymers (GFRP) and carbon-fibre reinforced polymers (CFRP), due to their high specific strength and stiffness, whilst comprising a low density. Their performance upon ageing and degradation, however, requires long-term verification and analyses [16].

Grogan et al. [17] implemented BEMT within a one-way fluid-structure interaction (FSI) model in analysing the structural response of slender tidal turbine blades. Solely utilising the thrust and tangential forces as the main sources of loading, the study compared the capacities of GFRPs and CFRPs under distinct load conditions. High bending moments under normal and extreme operating conditions were predicted to induce significant strains in GFRP spar caps, up to the point of fibre failure. Maximum strain levels in CFRP spar caps under similar loading conditions were found to be substantially reduced and well below the failure strain of the material.

Bir et al. [18] describe the structural design of a tidal turbine composite blade by FSI analysis. The hydrodynamic analysis was undertaken by means of BEMT, where the chord and twist pressure distributions were attained along the blade length, establishing the optimal performance of the tidal turbine over its lifetime. The extreme loads, i.e. the extreme flap and edgewise loads, induced upon the blade at extreme tidal flow conditions, were obtained utilising CFD. Subsequently, the outcomes of the structural analysis allowed the recognition of the optimal location of webs and the minimum thickness requirement of different composite laminates to satisfy the ultimate-strength and buckling-resistance criteria.

The numerical analysis elaborated in this present study is a continuation to Borg et al. [19] [20], in which a real-scale transient CFD model was developed to assess the hydrodynamic performance of a high-solidity open-centre tidal turbine within a bidirectional duct in aligned and yawed flows. This investigation furthers the study in analysing the structural response of the individual ducted turbine rotor blades succumb to aligned and yawed hydrodynamic flow. By utilising outcomes from the hydrodynamic blade-resolved CFD model, direct one-way coupling of the fluid-structure interaction was achieved. The hydrofoil geometry was provided by EDF R&D to replicate the outcomes of a turbine similar to the design of the OpenHydro PS2 device. In addition, the 7-equation RSM (Reynolds Stress Model) turbulence model was coupled to close the Reynolds-Averaged Navier-Stokes (RANS) equation, and analyse the flow domain.

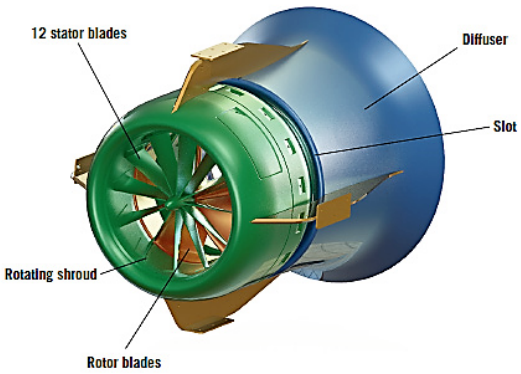

(a) Unidirectional duct [21]

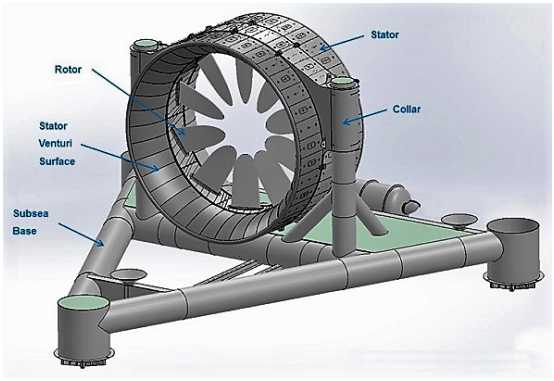

(b) Bidirectional duct [22]

Fig. 1: Illustrations of ducted tidal turbine installations

II. Numerical Methodology

A. Hydrodynamic Modelling

The computational fluid dynamic models were solved by means of ANSYS Fluent 18.0, where the physical models were designed to consist of a cuboidal domain layout, imposed with relevant boundary conditions. The CFD solver was utilised to compute the Reynolds-Averaged Navier-Stokes (RANS) equations as time-averaged representations of the continuity and momentum equations which govern the three-dimensional, unsteady, incompressible fluid flow. Slip wall or periodic conditions were instigated dependent on whether the analysis comprised of aligned flow or yawed flow. The domain surrounding the turbine was segregated from the global domain to induce a moving mesh model with rotation at the turbine. Turbulence was modelled by means of the RSM turbulence model due to its superiority in analysing anisotropic flows.

In a similar layout employed by Mason-Jones et al. [23], the dimensions of the computational domain were established to attain a maximum numerical blockage ratio of 2% with the turbine to ascertain the absence of far-field effects and replicate real-ocean conditions. This corresponded to cross-sectional domain dimensions of $7D$ at a length of $9D$, where the inlet and outlet were situated at a distance $3D$ upstream and $6D$ downstream of the turbine, respectively.

In an effort to attain a validated CFD model for tidal turbine applications, simulations were established to replicate the experimentation undertaken by Mycek et al. [24]. Identical blade, nacelle, and mast geometry were utilised within the model domain, onto which a tetrahedral mesh was imprinted. The general dimensions of the turbine include a diameter D of 0.7 m, a nacelle length of 2.5 m, and a mast length of 1 m, as illustrated in Fig. 2a (mast not included). The parameters of the turbine and fluid flow were also instated from the literature, with a free-stream velocity of 0.8 m/s and an inlet turbulence intensity of 3%. Upon validation, the model settings, identical to Borg et al. [19] were implemented for the analysis of a ducted eight-bladed tidal turbine, illustrated in Fig. 2b, similar to the design of the OpenHydro PS2 device. The general dimensions of the system include a turbine diameter of 12 m, a duct diameter of 15 m, and a duct length of 10 m. The turbine geometry was implemented within the model domain, onto which a tetrahedral mesh was imprinted. Similar to the validation, the physical model was designed to consist of identical domain layout and boundary conditions as the three-bladed HATT. The parameters of the turbine and fluid flow were instated from real-world data, provided by EDF R&D, where an aligned flow at 0^o, together with a yawed flow at an angle of 15^o, were considered.

A mesh independence procedure was carried out on the three-bladed HATT by considering the parameter with the highest degree of dynamics, which was the highest TSR condition. Subsequent to the procedure, the final surface mesh count utilised was marginally above 40,000 cells per blade, with dense volumetric cells around the turbine and within the wake, to achieve a total mesh count of 12 million for the three-bladed HATT, and 16 million for the ducted turbine. Fig. 3a presents an illustration of the ducted turbine surface mesh utilised for the CFD analysis. The final mesh was then implemented with an appropriate prism layer to achieve a y-plus value of $30 \leqslant y^+ \leqslant 500$ across the blades and duct.

The CFD computations were performed using the ARCHIE-WeSt cluster facility at the University of Strathclyde by running two Intel Xeon Gold 6138 2.00 GHz computational nodes, with 40 cores and 192 GB of RAM per node per simulation. The ducted turbine simulations were completed within roughly 75 wall-clock hours, equivalent to 3,000 core-hours, hence resulting in 5 wall-clock hours per turbine rotation.

B. Structural Modelling

The finite element method (FEM) models were solved by means of ANSYS Mechanical APDL 18.0, where the physical models were designed to explicitly contain all eight blades, imprinted with a hybrid hexahedral/tetrahedral mesh consisting of solid quadratic elements, illustrated in Fig. 3b, imposed with relevant boundary conditions.

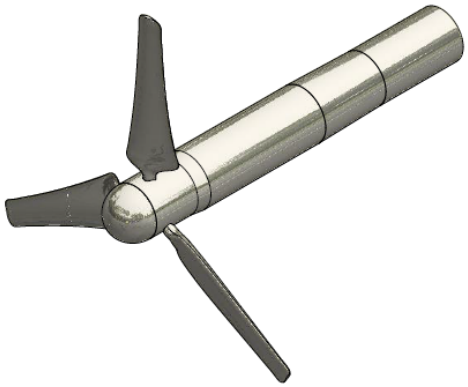

(a) Representation of the Three-Bladed HATT [19]

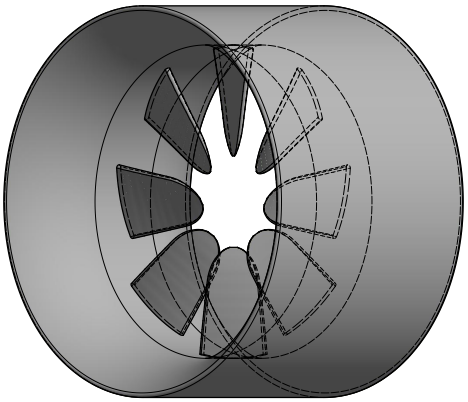

(b) Representation of the Ducted High-Solidity Tidal Turbine

Fig. 2: CAED Illustrations of the simulated turbines

The FEM solver was utilised to implicitly compute the dynamic representations of the linear elastic relationship for the isotropic and anisotropic composite materials. The loading conditions were implemented directly as distributions of pressure from the CFD solver at distinct temporal points. This setup hence allows an isolated blade-resolved fluid-structure interaction analysis to be undertaken, as each blade is independent from the entire system, upon which unique loading conditions are induced. The surface of the blade utilised in the FEA analysis is directly replicated from the CFD analysis, which numerically represents the actual fabricated blades protruding from the duct housing. For this reason, the segment of the blades solely succumb to the hydrodynamic flow was structurally modelled; in this circumstance, however, true structural replication is not put forward. In this respect, the surface directly attached to the duct was not allocated with a fixed condition in all axes, yet applied with a spring constant along the perimeter of the surface, allowing limited movement up to a maximum of 0.05 m in the axial axis, in assumption

TABLE I: Material properties adopted in the structural numerical model [17]

Material	E_1 (GPa)	E_2 (GPa)	G_{12} (GPa)	ν_{12}	Density (kgm^{-3})	Design
DB GFRP	22.0	22.0	2.7	0.30	1850	Solid
UD GFRP	38.8	10.0	2.7	0.30	1950	Cored
Corecell	0.044	0.044	0.020	0.30	65	Cored

of the tolerance allowed between the physical surfaces of the blade and the duct, with a fixed condition disallowing motion in the radial and tangential axes.

In an effort to acquire an efficacious turbine design in terms of blade performance, material properties, and cost-effectiveness, two design variations were considered: a solid blade consisting of a single material and a cored blade consisting of a shell filled with a foam core, in replication of turbine blades elaborated in [25]. The composite materials properties utilised were double-biased (DB) glass-fibre reinforced polymers (GFRP) for the solid blade analysis, and a uni-directional (UD) glass-fibre reinforced polymers with structural foam at the core for the cored blade, where the criteria of the analysis, related to blade axial deformation, induced radial strains, and rotor specific mass, allowed a definitive selection of the more applicable implementation. The structural properties of the aforementioned materials are presented in Table I.

III. Model Characterisation

In consideration of the analysis of a physical turbine, notable definitions concerning the resultant performance outcomes, in terms of the boundary conditions employed, are identified. Utilised to attain quasi-real-ocean conditions, the blockage ratio (α_{bl}) is defined as a correlation between the device reference area (A_{dvc}) and the domain sectional area (A_{dmn}):

$$\alpha_{bl} = \frac{A_{dvc}}{A_{dmn}} = \frac{\pi R_{dvc}^2}{L_{dmn}^2} \tag{1}$$

where R_{dvc} is the device radius, and L_{dmn} is the length of the quadratic cross-sectional area of the computational domain.

The tip speed ratio (TSR) is established as an equivalence between the linear blade-tip velocity and the free-stream velocity:

$$TSR = \frac{|\Omega_{sys}|R_{rtr}}{U_\infty} = \frac{|\Omega_x|R_{rtr}}{U_\infty} \tag{2}$$

where Ω_{sys} is the system rotational speed, hence Ω_x being the axial angular velocity, U_∞ is the free-stream velocity, and R_{rtr} is the rotor radius. A distinction must be made between the device radius and the rotor radius when modelling ducted turbines. In the case of a ducted turbine, $R_{dvc} \neq R_{rtr}$, but $R_{dvc} = R_{dct}$, contrary to a non-ducted turbine, where $R_{dvc} = R_{rtr}$.

To determine the turbine capacity in converting the fluid free-stream energy into rotational energy, the power coefficient (C_P) is established. This considers the mechanical rotational power attained by the device (P_{dvc}) as a ratio of the maximum rotational power potentially acquired in the device area (P_∞):

$$C_P = \frac{P_{dvc}}{P_\infty} = \frac{M_x\Omega_x}{\frac{1}{2}\rho A_{dvc}U_\infty^3} = \frac{M_x\Omega_x}{\frac{1}{2}\rho\pi R_{dvc}^2U_\infty^3} \tag{3}$$

where M_x is the axial moment, also referred to as the rotor torque.

In ascertaining the forces induced on the turbine, the thrust coefficient (C_T) is established. This considers the drag force on the device (F_{dvc-x}) as a ratio of the related force on the device area ($F_{\infty-x}$):

$$C_T = \frac{F_{dvc-x}}{F_{\infty-x}} = \frac{F_{dvc-x}}{\frac{1}{2}\rho A_{dvc}U_\infty^2} = \frac{F_{dvc-x}}{\frac{1}{2}\rho\pi R_{dvc}^2U_\infty^2} \tag{4}$$

To establish the structural response of the blade, the axial deflection coefficient (δ_z^*) was defined as the physical axial deflection (δ_z) in relation to the rotor geometry:

$$\delta_z^* = \frac{\delta_z}{R_{rtr}} \tag{5}$$

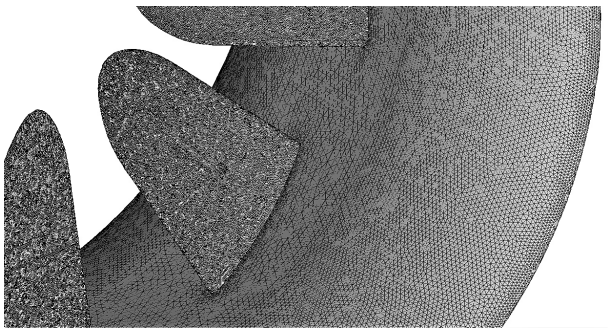

(a) Illustration of the ducted turbine surface mesh utilised for CFD analysis

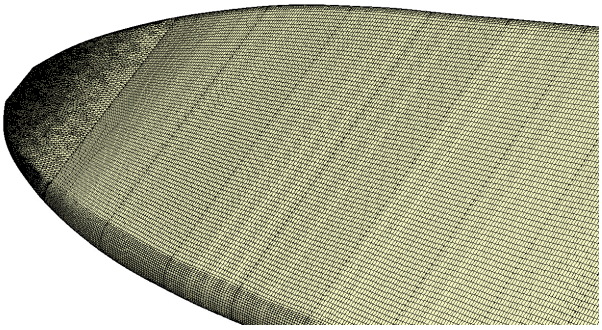

(b) Illustration of the blade surface mesh utilised for FEA analysis

Fig. 3: Illustrations of the meshes utilised for the fluid-structure interaction framework

IV. Results & Discussion

Consequent to the methodology, the resultant outcomes, in terms of power coefficient, thrust coefficient, and velocity profiles in the wake, were established for the validation case. As elaborated upon in the previous study [19], the three-bladed HATT CFD model outcomes were compared to the

literature [24] introduced above. In correlating the distinct performance curves, a total similarity of 95.52% was acknowledged at the power coefficient plateau region (TSR 3.6 - 6.2), together with all CFD data points falling within $2\sigma_{C_P}$ with experimentation data points, hence within the 95^{th} percentile, displaying good comparison.

In accordance to the validated CFD model, the resultant outcomes, in terms of the power coefficient and thrust coefficient were established for the ducted tidal turbine simulation cases in aligned and yawed flow.

A. Power Analysis

Primarily, the resultant power coefficient variation between the yaw angles was established. Illustrated in Fig. 4, both the trend and values attained in the power curve vary significantly between aligned flow and yawed flow. Notably, when succumb to aligned flow, the TSR curve is relatively short spanning, with a TSR range of 1 - 2.5, which is characteristic of a high-solidity turbine. Within this region, a high gradient power increase towards a maximum power coefficient of 0.345 at a TSR of 1.75 was acknowledged, followed by a steep decrease to a decrease of 0.1 from its nominal TSR.

The more notable distinction is the increase in power coefficient at a yaw angle of 15^o within higher TSRs (2.0 - 2.5). Literature [6] has speculated the diminishment of the power coefficient of an HATT upon different bearings of yawed flow, resulting in a turbine to become less effective in accordance with the yaw angle. Current data contemplates the effectivity of the installation of a shroud, as a result of an imposed alignment of the flow at the turbine, marginally surpassing the maximum power coefficient in aligned flows. A more steady power gradient increase was attained at the yaw angle through this range, with a sudden spurt at nominal TSR, which shifts to a value of 2.0, to a maximum power coefficient of 0.346. An increase in global power within the analysed TSR range was also developed, with a 2.68% increase in the integral of the torque coefficient with TSR.

B. Thrust Analysis

Having considered the variation in power generated by means of an introduction of angular flow, the disparity in thrust was analysed in accordance to the flow bearing. Illustrated in Fig. 5, the depiction ascertains a substantial variation in the force induced upon the turbine system due to the fluid-structure interaction. At aligned flows, the thrust decreases from a substantially high value of 1.16 at low TSR to 1.01 at nominal TSR, at which the gradient of decline increases, to a coefficient of 0.69 at high TSR. Under yawed flows, at a bearing of 15^o, the resultant thrust is lesser than that within aligned flows, a result of the misalignment of the flow, as a vectorial component of the free-stream acts perpendicular to the direction of the turbine central axis. This lessened force induction, however, solely acts up to the nominal TSR, after which, albeit sustaining diminishment, attains higher values when compared to thrust at aligned flows. This increase in thrust is attributable to the preservation of the pressure

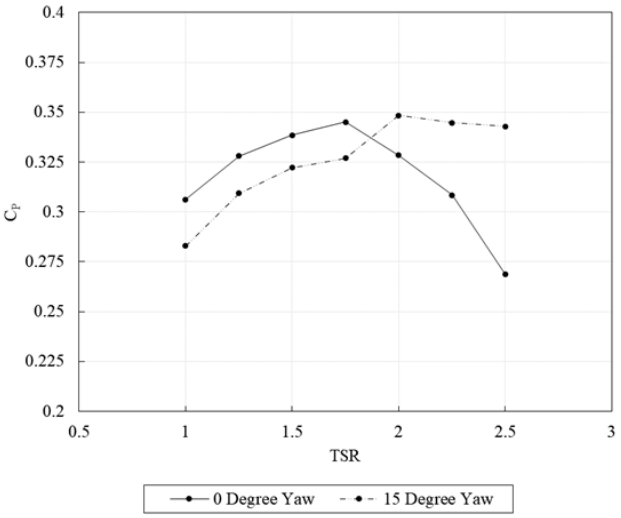

Fig. 4: Comparison of the Power Coefficient for the Ducted Turbine in Aligned and Yawed Flows

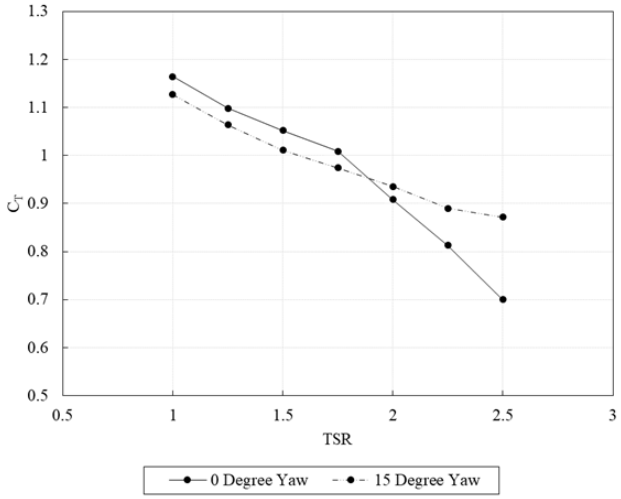

Fig. 5: Comparison of the Thrust Coefficient for the Ducted Turbine in Aligned and Yawed Flows

difference at high TSRs, which directly induces the drag at the turbine structure.

C. Structural Analysis

Having acknowledged the fluid dynamic performance characteristics of a high-solidity tidal turbine, the resultant structural response due to the pressure distribution along the blade induced by the hydrodynamic flow was deduced. In effort of establishing an appropriate design for the high-solidity blades, two setups were considered, a solid blade and a cored blade, evaluated upon criteria that include the axial deflection of the blades, the developed radial strain, and the specific mass of the rotor.

In analysing the axial deflection of the blades, the relation with TSR was acknowledged to act in a similar manner as

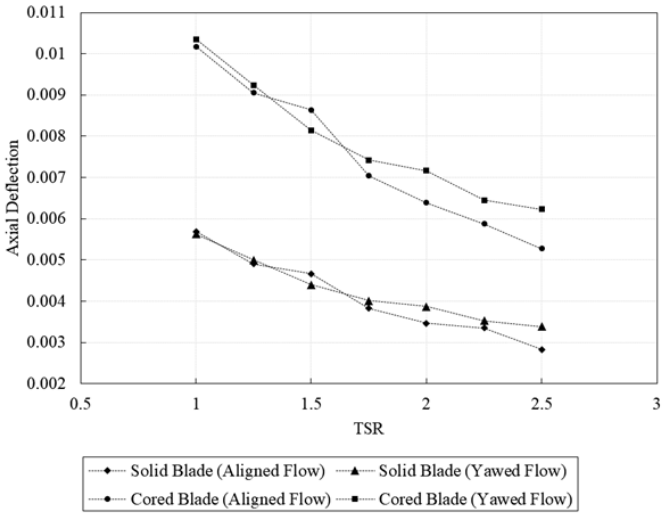

Fig. 6: Comparison of the Axial Deflection Coefficient for the Ducted Turbine Blades in Aligned and Yawed Flows

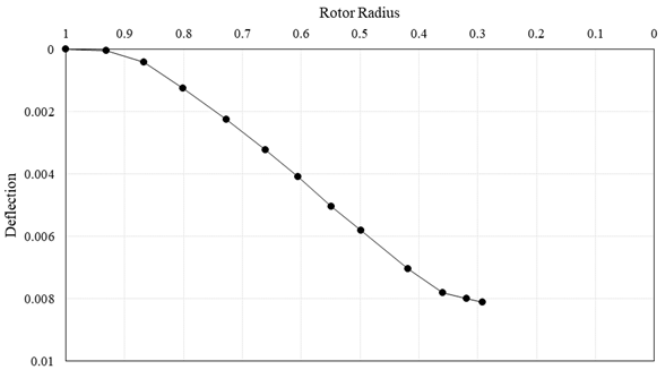

Fig. 7: Beam Mid-Plane Deflection Curve of the High-Solidity Turbine Blade (cored blade within yawed flow at TSR 1.50)

the thrust coefficient, a negatively proportional affiliation, as illustrated in Fig. 6. As depicted, the cored blades undergo higher deflection as a result of the hydrodynamic flow due to the implementation of the foam core, which constitutes more than 80% of the blade volume, diminishing the global Young's modulus, and hence, rigidity. Albeit the higher deflection, the axial deflection is relatively insubstantial for both designs, with a maximum deflection equal to 0.0102 of the rotor radius, roughly equivalent to a deflection angle of 1.09^o. This minute deflection comes about as the blade is constrained at its tip, where the higher forces are induced, rather than at the hub.

When comparing aligned flow deflections to those under yawed flow, the deflections of the blade at higher TSRs are larger for yawed flows; this matches with the variation in thrust under the same conditions. The behaviour of the deflection down the blade was investigated, attaining its maximum value at the trailing edge towards the tip of the blade, as illustrated

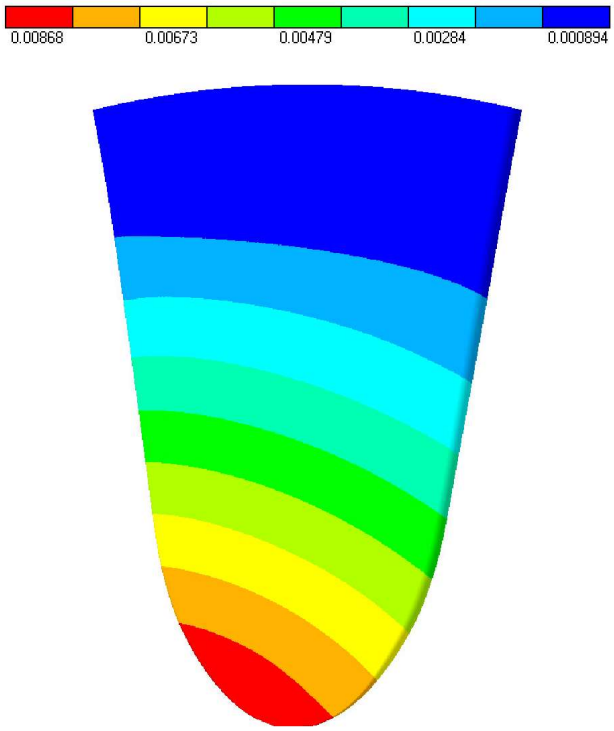

Fig. 8: Illustration of Axial Deflection of the High-Solidity Blade (cored blade within yawed flow at TSR 1.50)

in Fig. 8, yet not at the outermost extremity of the tip as in the theoretical response of a cantilever beam. This is due to the variation in the cross-sectional profile of the blade, together with the twist imposed through the structure. Inspecting the deflection within one-dimensional beam displacement down the mid-plane section of the blade, depicted in Fig. 7, in fact produces the typical cantilever response.

In consequence of its considerable frontal area and narrow form, whilst being fixed at a boundary, the high-solidity blade acts with structural responses of both a shell and a cantilever beam. For reason of being susceptible to high bending and shear strain, hence failure induced via fibre elongation, the maximum radial strain induced within the thin GFRC structure, depicted in Fig. 9, was established. Proportional to the variation in blade deflection, and hence, thrust induced upon the blade, the radial strain within the blade diminishes with TSR, and was found to be more substantial within the cored blade due to the comparably lesser rigidity. Albeit the strain, the maximum value does not exceed the ultimate strain value of the GFRC simulated, and hence, is within the limits of reliable operation. A notable outcome, however, is the distribution of the radial strain within the blade. Illustrated in Fig. 10, a strain concentration is present at the leading edge of the blade, within the vicinity of the root, occurring along both the solid and cored blades, in both aligned and yawed flows. In consequence of the presence of a stress localisation, if a structural defect were to transpire, such as a crack, propagation

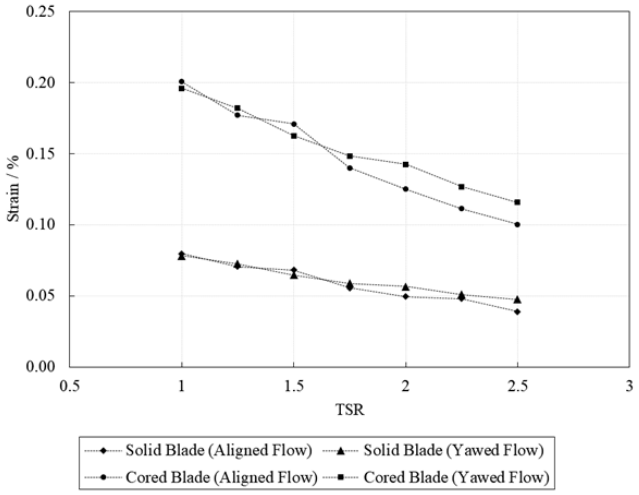

Fig. 9: Comparison of the Radial Strain for the Ducted Turbine Blades in Aligned and Yawed Flows

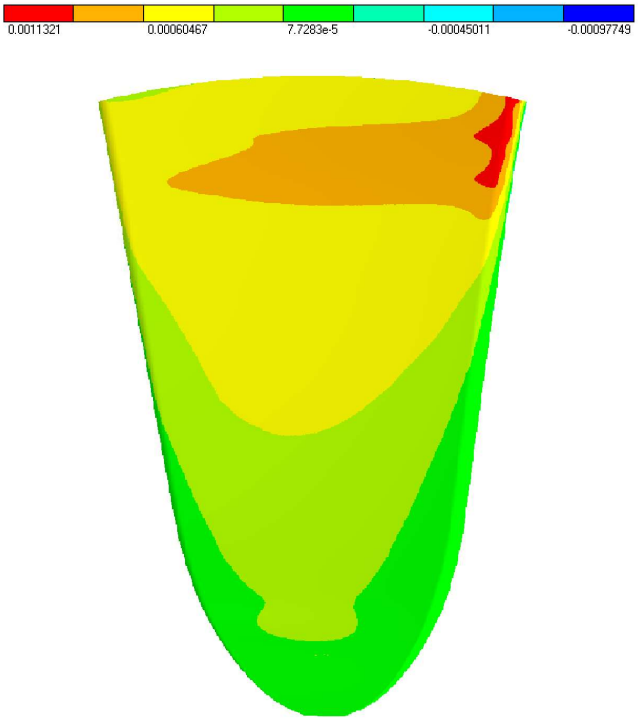

Fig. 10: Illustration of Radial Strain Distribution along the Upstream Surface of the High-Solidity Blade (cored blade within aligned flow at TSR 2.25)

of that defect may ensue, resulting in the structural failure of the high-solidity blade. This concentration is brought about due to the simultaneous bending and torsion instigated by the fluid-structure interaction on the narrow blade.

In consideration of the relatively comparable structural outcomes, the specific mass of the two rotor designs was established; the solid blade was found to attain a value of 1850 kg/m^3, whilst the cored blade was found to attain a value of 409.5 kg/m^3, a 77.86% difference. As a lower resultant moment of inertia facilitates the rotational acceleration of the rotor at operational start-up, the cored blade provides an efficacious setup to the solid blade. The full usage of the interior blade volume to be filled with structural foam, however, was found to be superfluous, in addition to the implementation of unidirectional fibres, rather than a double bias layout, arguably inducing higher manufacturing costs. Hence, albeit the favourable combination of rigidity and unsubstantial weight, a more efficacious design may be investigated to pursue a more appropriate implementation.

V. Conclusion

Efforts in increasing the efficiency of energy-generating turbines will persevere with pushing the boundaries of offshore technologies. This study has elaborated a one-way fluid-structure interaction numerical model utilised in investigating the structural mechanics concerning the rotor blades comprising a ducted high-solidity tidal turbine. Coupling hydrodynamic outcomes as structural inputs in effort of acknowledging the most applicable setup, distinct designs were investigated, solid blades and cored blades, analysed within criteria related to blade axial deformation, induced radial strains, and rotor specific mass.

The outcomes depicted approximately double the axial deflection for a cored blade, with four times the degree of strain, in comparison to a solid blade. This discrepancy came about due to the decreased rigidity of the prior design, with the use of a less strong material within the interior of the blade, which resulted in its specific mass to decrease by a factor of roughly 4.5. In consideration that the blade response of the cored design is within its structural property limits, in addition to being lighter, together with inducing substantial rigidity, hence sustaining its hydrodynamic performance characteristics within a quasi-rigid structure assumption, the cored blade was established to be the preferred design.

Acknowledgments

The research work disclosed in this publication is partially funded by the Endeavour Scholarship Scheme (Malta). Scholarships are part-financed by the European Union – European Social Fund (ESF) – Operational Programme II – Cohesion Policy 2014-2020: *"Investing in human capital to create more opportunities and promote the well-being of society"*.

Results were obtained using ARCHIE-WeSt High Performance Computer (www.archie-west.ac.uk).

References

[1] P. Gipe, "WIND-WORKS: Ducted Wind Turbines," 2018.
[2] Bloomberg L.P., "OpenHydro Group Limited: Private Company Information - Bloomberg," 2018.
[3] OpenHydro Group Ltd., "Projects," 2016.
[4] M. J. Werle and W. M. Presz, "Ducted Wind/Water Turbines and Propellers Revisited," *Journal of Propulsion and Power*, vol. 24, pp. 1146–1150, 9 2008.

[5] C. F. Fleming and R. H. Willden, "Analysis of bi-directional ducted tidal turbine performance," *International Journal of Marine Energy*, vol. 16, pp. 162–173, 2016.

[6] C. S. Belloni, R. H. Willden, and G. T. Houlsby, "A Numerical Analysis of Bidirectional Ducted Tidal Turbines in Yawed Flow," *Marine Technology Society Journal*, vol. 47, pp. 23–35, 7 2013.

[7] S. Allsop, C. Peyrard, P. R. Thies, E. Boulougouris, and G. P. Harrison, "Hydrodynamic analysis of a ducted, open centre tidal stream turbine using blade element momentum theory," *Ocean Engineering*, vol. 141, pp. 531–542, 9 2017.

[8] M. Shives, C. Crawford, and S. Grovue, "A tuned actuator cylinder approach for predicting cross-flow turbine performance with wake interaction and channel blockage effects," *International Journal of Marine Energy*, vol. 18, pp. 30–56, 6 2017.

[9] U. Ahmed, D. Apsley, I. Afgan, T. Stallard, and P. Stansby, "Fluctuating loads on a tidal turbine due to velocity shear and turbulence: Comparison of CFD with field data," *Renewable Energy*, vol. 112, pp. 235–246, 11 2017.

[10] M. A. Holst, O. G. Dahlhaug, and C. Faudot, "CFD Analysis of Wave-Induced Loads on Tidal Turbine Blades," *IEEE Journal of Oceanic Engineering*, vol. 40, pp. 506–521, 2015.

[11] C. Schulz, P. Letzgus, T. Lutz, and E. Kramer, "CFD study on the impact of yawed inflow on loads, power and near wake of a generic wind turbine," *Wind Energy*, vol. 20, pp. 253–268, 7 2016.

[12] M. Suzuki, "Numerical Analysis of Horizontal-Axis Wind Turbine Characteristics in Yawed Conditions," *Open Journal of Fluids Mechanics*, vol. 2, pp. 331–336, 12 2012.

[13] M. K. McWilliams, S. Lawton, S. Cline, and C. Crawford, "A Corrected Blade Element Momentum method for Simulating Wind Turbines in Yawed Flow," in *49th AIAA Aerospace Sciences Meeting including the New Horizons Forum and Aerospace Exposition*, (Orlando, Florida), AIAA, 2011.

[14] J. Morote, "Angle of attack distribution on wind turbines in yawed flow," *Wind Energy*, vol. 19, pp. 681–702, 6 2015.

[15] A. Munoz, L. Chiang, and E. De la Jara, "A design tool and fabrication guidelines for small low cost horizontal axis hydrokinetic turbines," *Energy for Sustainable Development*, vol. 22, pp. 21–33, 5 2014.

[16] P. Harper and S. Hallett, "Advanced numerical modelling techniques for the structural design of composite tidal turbine blades," *Ocean Engineering*, vol. 96, pp. 272–283, 12 2015.

[17] D. Grogan, S. Leen, C. Kennedy, and C. Bradaigh, "Design of composite tidal turbine blades," *Renewable Energy*, vol. 57, pp. 151–162, 9 2013.

[18] G. S. Bir, M. J. Lawson, and Y. Li, "Structural Design of a Horizontal-Axis Tidal Current Turbine Composite Blade," in *ASME 30th International Conference on Ocean, Offshore, and Arctic Engineering*, (Rotterdam, Netherlands), ASME, 2011.

[19] M. G. Borg, Q. Xiao, A. Incecik, S. Allsop, and C. Peyrard, "Numerical Analysis of a Ducted High-Solidity Tidal Turbine," in *OCEANS'18 MTS/IEEE Kobe*, (Kobe, Japan), IEEE, 2018.

[20] M. G. Borg, Q. Xiao, A. Incecik, S. Allsop, and C. Peyrard, "An Actuator Disc Analysis of a Ducted High-Solidity Tidal Turbine in Yawed Flow," in *ASME 2019, 38th International Conference on Ocean, Offshore, and Arctic Engineering, OMAE 2019*, (Glasgow, Scotland), ASME, 2019.

[21] R. Billett, "Rising Tide," *ANSYS Advantage*, vol. IX, pp. 25–27, 2015.

[22] Crist Offshore, "Open-Centre Tidal Turbine," 2015.

[23] A. Mason-Jones, D. M. O'Doherty, C. E. Morris, T. O'Doherty, C. B. Byrne, P. W. Prickett, R. I. Grosvenor, I. Owen, S. Tedds, and R. J. Poole, "Non-Dimensional Scaling of Tidal Stream Turbines," *Energy*, vol. 44, pp. 820–829, 2012.

[24] P. Mycek, B. Gaurier, G. Germain, G. Pinon, and E. Rivoalen, "Renewable Energy Experimental study of the turbulence intensity effects on marine current turbines behaviour. Part I: One single turbine," *Renewable Energy*, vol. 66, pp. 729–746, 2014.

[25] L. Krstulovic-Opara, B. Klarin, and Z. Domazet, "A non-destructive wind turbine blade analysis based on the Thermal Stress Analysis," (Split, Hrvatska), 2009.